Crystal-field spectrum in $RBa_2Cu_3O_x$ (R = Er, Ho) high-T_c superconductors: evidence for charge order in CuO_2 planes

1999 J. Phys.: Condens. Matter 11 7155

(http://iopscience.iop.org/0953-8984/11/37/312)

J. Phys.: Condens. Matter **11** (1999) 7155–7173. Printed in the UK PII: S0953-8984(99)01464-2

Crystal-field spectrum in $RBa_2Cu_3O_x$ (R = Er, Ho) high-T_c superconductors: evidence for charge order in CuO_2 planes

A Mirmelstein†, A Podlesnyak, V Bobrovskii and I Zhdakhin

Institute for Metal Physics, Russian Academy of Science, 620219 Ekaterinburg GSP-170, Russia

E-mail: alex@sobos.e-burg.su (A Mirmelstein)

Received 1 February 1999, in final form 13 May 1999

Abstract. A model of the crystal field generated by a periodic array of charged tapes is developed to analyse the crystal-field interaction in $RBa_2Cu_3O_x$ (R = Er, Ho) high-T_c copper oxides observed by the inelastic neutron scattering technique. The explicit calculation of the parameters of the Stevens Hamiltonian describing crystalline electric field effects in solids is performed for a specific charge density distribution uniformly extended in a certain direction of the crystal lattice. The model accounts for the x-dependence of the crystal-field parameters and allows us to determine the hole concentration in the CuO_2 planes as a function of oxygen stoichiometry. The model of the periodic array of charged tapes suggests a charge order induced in the CuO_2 planes by doping.

1. Introduction

Despite essential progress gained in understanding of the properties of copper oxide superconductors since their discovery [1], basic features of the electronic states of these layered compounds are still widely debated. Different scenarios [2–12] have been suggested to explain the origin of the pseudogap [13–19] and, in general, the development of the electronic properties across the phase diagram of cuprates. Inhomogeneous charge distribution resulting from doping of antiferromagnetic parent compounds with charge carriers is of particular interest. It has been theoretically shown that dilute holes in a layered antiferromagnet can be unstable against phase separation into hole-rich and hole-poor regions at intermediate length scales [2–7]. At the same time there is growing experimental evidence for mesoscopic striped phases and their effect on the electronic properties in perovskite materials [20–29]. It is therefore of crucial interest to obtain direct experimental information on charge distribution within the superconducting CuO_2 planes of high-T_c cuprates. Since in most rare-earth based high-T_c compounds the R ions are situated close to the CuO_2 planes, the crystalline electric field (CEF) interaction at the R site constitutes an ideal probe of the local symmetry as well as the local charge distribution, and thereby directly monitors the variation of the carrier concentration induced by doping [30]. The inelastic neutron scattering technique (INS) is a valuable tool to investigate the CEF excitations in optically opaque high-T_c compounds. This technique allowed unique experimental information to be obtained on the peculiarities of the charge transfer process and the cluster formation upon doping (which may be called 'frustrated phase separation') as well as on the symmetry of the gap function of high-T_c superconductors [30–32].

† Corresponding author: Institute for Metal Physics, Russian Academy of Science, 18, S Kovalevskaya Street, 620219 Ekaterinburg GSP-170, Russia.

0953-8984/99/377155+19$30.00

In spite of these achievements a quantitative analysis of the doping dependence of the crystal-field parameters for CEF spectra of rare-earth ions dissolved in high-temperature superconductors remains unsatisfactory. This is due to the lack of better approaches for the crystal-field effects in solids than those based on the point charge (PC) model.

In the present paper a new approach is developed to describe the variation of the CEF parameters versus oxygen stoichiometery in high-temperature superconductors of the type $RBa_2Cu_3O_x$ (R = Er, Ho), so far the most studied by the INS technique from the point of view of experimental completeness and precision. This approach is based on the consideration of the periodic array of charge tapes induced in the CuO_2 planes by hole doping. The explicit calculation of the parameters of the crystal-field Hamiltonian (in the form of the Stevens operator equivalents [33, 34]) is given for such an extended charge geometry. It is shown that the model is able to explain the experimentally observed changes of the CEF parameters in $RBa_2Cu_3O_x$ (R = Er, Ho) and allows us to determine the hole concentration in the CuO_2 planes as a function of x. The formation of the periodic array of charged tapes provides evidence for a charge order occurring in the CuO_2 planes due to doping. However, this order cannot directly be identified with charge stripes widely discussed from both theoretical [2–7] and experimental sides [20–29].

2. CEF spectra in $ErBa_2Cu_3O_x$ copper oxide

In $ErBa_2Cu_3O_x$ the crystal field splits the ground-state J-multiplet $^4I_{15/2}$ of the Er^{3+} ions into eight Kramers doublets. Three CEF levels A, B, C were found in a low-energy window ($\Delta E < 12$ meV) and four levels D, E, F, G in a high-energy window ($65 < \Delta E < 82$ meV) [31]. The effect of increase in oxygen content is a shift of the CEF level A to higher energy and increase of its intensity and a subtle shift of the levels F and G up and lines B, D and E down. The energy of the transition C remains unchanged. Considering energies and relative intensities of seven CEF transitions a set of nine CEF parameters B_{nm} ($n = 2, 4, 6$; $m = 0, 2, \ldots, n$) can be derived for each oxygen concentration [31]. Figure 1(a) shows that parameter B_{20} varies by a factor of two when going from $x = 6$ to $x = 7$. The leading fourth- and sixth-order parameters B_{nm} ($n = 4, 6$; $m = 0, 4$) undergo rather small changes within a few percent. As a result, the main features of the x-dependence of the CEF spectrum in $ErBa_2Cu_3O_x$, both line energies and intensities, could be reproduced by the variation of B_{20} alone keeping all the other CEF parameters fixed. Figure 2 displays this behaviour in the low-energy window (for more details see [30–32]). Increase in B_{20} corresponds to increase in x. Experimentally, B_{20} varies from 6.3 to 14 meV for $6 < x < 7$. Note, that for convenience here and below we use the notations in which reduced matrix elements $\Theta_n = 1$, i.e. $B_{nm} = B_{nm}(\text{Stevens})/\Theta_n$.

As demonstrated in detail for $RBa_2Cu_3O_x$ [31, 35], the CEF interaction is mainly determined by the position and the charges of the oxygen ions in the CuO_2 planes. Respectively, the variation of the leading fourth- and sixth-order CEF parameters can only be interpreted as a result of an increase of the hole concentration in the CuO_2 planes due to doping. In order to quantify this result the following modified point-charge relation was suggested [31, 36]:

$$B_{nm}(x)/B_{nm}(7) = [1 + \delta(x)]\gamma_{nm}(x)/\gamma_{nm}(7) \tag{1}$$

where $\delta(x)$ is the relative charge transferred from the chains to the planes (in units of the electron charge $|e|$). The compound $ErBa_2Cu_3O_7$ is taken as a reference, i.e. $\delta(7) = 0$. The geometrical coordination factors γ_{nm} are calculated in the PC approximation [33] for the nearest-neighbour oxygen polyhedron formed by the in-plane O(2) and O(3) ions. Oxygen positions are assumed to be known from neutron diffraction measurements. Equation (1) gives $\delta \approx 0.28$ holes/(unit cell) in $RBa_2Cu_3O_x$ (R = Er, Ho) for x varying from 6 to 7 [31],

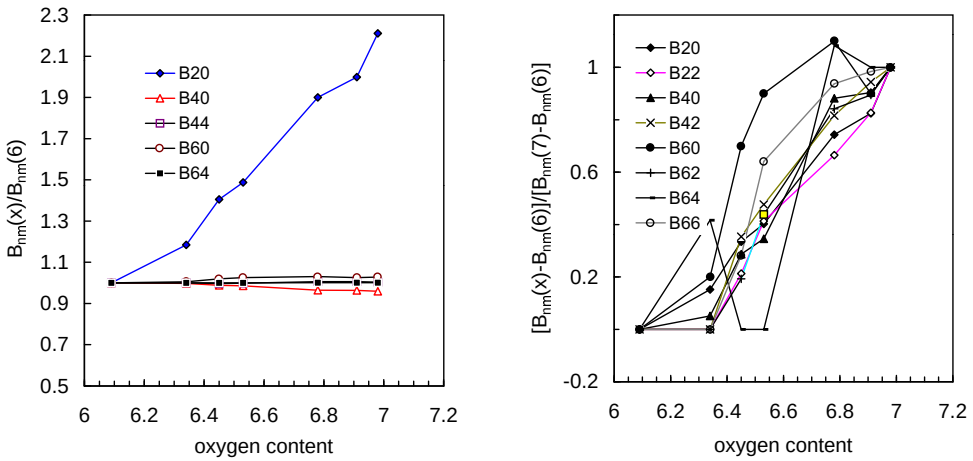

Figure 1. (a) Relative variation of the leading CEF parameters as a function of x for $ErBa_2Cu_3O_x$ derived from inelastic neutron scattering experiments [31]. (b) The same data plotted as normalized increment of the CEF parameters versus oxygen content. 'Orthorhombic' parameters ($m = 2, 6$) are also included. B_{44} is not shown because of large scattering of experimental points.

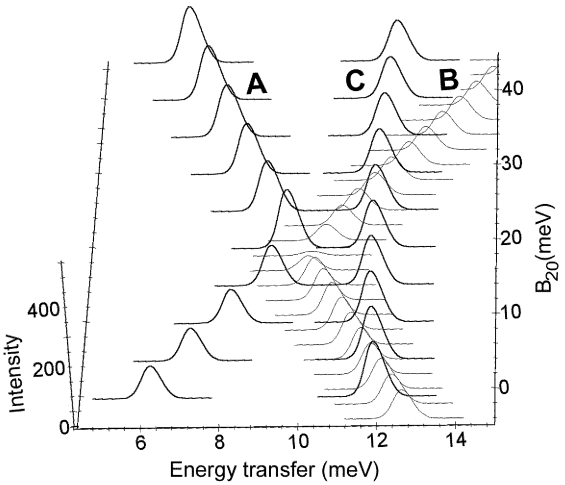

Figure 2. Numerical simulation of the CEF spectrum for $ErBa_2Cu_3O_x$ as a function of B_{20} parameter alone. All other CEF parameters are fixed at their values for $x = 6.09$ [31]. The plot reproduces the main features of the observed behaviour. Experimentally, B_{20} varies from 6 to 14 meV for x going from 6 to 7.

i.e. very close to the generally accepted value of the hole concentration at optimal doping [37]. The second order parameter B_{20} cannot be described by such a simple relation despite the fact that normalized increments of all the CEF parameters, both 'tetragonal' ($m = 0, 4$) and 'orthorhombic' ($m = 2, 6$), display the same trend (figure 2(b)). Such a behaviour suggests that the actual doping-induced charge geometry in the CuO_2 planes cannot be approximated by point charges.

Table 1. Calculated CEF parameters for $ErBa_2Cu_3O_x$. The algorithm takes into account corrections for shielding by the outer shells [39] and screening due to charge carriers [40] ($k = 0.73$ Å) as described in the text (see also [30]). Crystallographic parameters of the lattice for $x = 6.98$ and 6.09 as well as the observed values of the CEF parameters are taken from [31]. $Z[O(i)]$ is the charge of the oxygen ions in the plane ($i = 2, 3$) and chain ($i = 4$) positions. The notation is used in which reduced matrix elements $\Theta_n = 1$. Recalculation to the Stevens formalism is given by $B_{nm}(\text{Stevens}) = B_{nm}\Theta_n$.

(n, m)	$x = 0.69$ (observed)	$x = 6.98$ (observed)	$x = 6.98$ $Z[O(2)] = -2$ $Z[O(3)] = -2$ $Z[O(4)] = -2$	$x = 6.98$ $Z[O(2)] = -1.92$ $Z[O(3)] = -1.92$ $Z[O(4)] = -2$	$x = 6.09$ $Z[O(2)] = -2$ $Z[O(3)] = -2$ $Z[O(4)] = 0$
(2, 0)	6.30(22)	13.93(73)	15.4	15.3	16.9
(2, 2)	0	11.64(3.1)	12.4	11.9	0
(4.0)	−33.61(11)	−32.25(19)	−29.0	−27.8	−29.1
(4, 2)	0	10.26(3.2)	9.73	9.36	0
(4.4)	156.31(66)	156.81(1.42)	157.7	152.0	158.4
(6, 0)	3.57(2)	3.67(6)	3.3	3.1	3.1
(6, 2)	0	−0.57(15)	−2.3	−2.3	0
(6, 4)	104.47(11)	104.59(27)	103.4	99.9	103.2
(6, 6)	0	0.64(14)	1.2	1.2	0

Limitation to use the PC approximation for $RBa_2Cu_3O_x$ does not result from the consideration of the nearest-neighbour oxygen polyhedron. The CEF parameters for metallic perovskites can be calculated using an *ab initio* method suggested by Mesot and Furrer [30]. In this method a finite cluster of the $ErBa_2Cu_3O_7$ crystal is considered which includes neighbouring ligand shells up to 10 Å out of Er^{3+} site. All ions within this sphere are taken into account with their nominal charges. Following Sternheimer [38] and Morrison [39], corrections for shielding effects are included. The screening effect due to charge carriers is taken into account by a Yukawa-type potential [40]. Using the crystal structure parameters of $ErBa_2Cu_3O_{6.98}$ from [31] and by adjusting the screening length $k = 0.73$ Å, the CEF parameters were calculated and found to be reasonably close to the experimental values (table 1). However, this *ab initio* cluster calculation cannot reproduce the x-dependence of the CEF parameters, especially B_{20}. Variation of the charges of O(2) and O(3) ions in the CuO_2 planes (replacing $Z[O(2), O(3)] = -2$ by $Z = -1.92$, as follows from the estimated charge transfer in terms of equation (1) [31]) causes a very small change of the CEF parameters (table 1). Similarly, the observed variation of the CEF parameters with x cannot be described by removing oxygen ions from the O(4) sites and by taking into account the corresponding structural variation. In the frame of this cluster calculation the decrease in B_{20} for x going from 7 to 6 can only be achieved by the decrease of the screening length. Obviously, such an assumption is not acceptable. First, the screening length is expected to grow in an insulating state. Second, an essential variation of the screening length required to decrease B_{20} by a factor of two will immediately change fourth- and sixth-order CEF parameters, in disagreement with the experiment.

A certain restriction to use the PC approximation for the quantitative analysis of the CEF effects in $RBa_2Cu_3O_x$ follows directly from the INS experiment. A rather strong disorder, introduced into Er-'123' by means of fast neutron irradiation at liquid nitrogen temperature has been shown to result only in the broadening of the CEF lines due to static atomic displacements [41]. Since the CEF splitting does not change and the crystal lattice parameters grow essentially, in terms of the PC model this would imply a disorder-induced increase of the charge in the CuO_2 planes. Such a conclusion disagrees with other experimental data [41].

Since the experimental results strongly suggest that the CEF spectrum in Er-'123' is determined by charge states in the CuO_2 planes, it seems reasonable to directly relate the variation of the charge state within the CuO_2 planes due to hole doping with the observed behaviour of the CEF parameters. The model described in the next section was developed to solve this problem.

3. Model of extended planar charge structure

It is common in solid-state physics to describe crystalline electric field effects due to point charges by parameters of the so-called Stevens Hamiltonian (SH) [33, 34, 42]. However, the form of the SH is not restricted by the point character of the charges. Therefore, the general method to calculate the SH coefficients [33] can be adapted for any charge geometry, e.g. for a specific charge distribution uniformly extended in a certain direction of the crystal lattice.

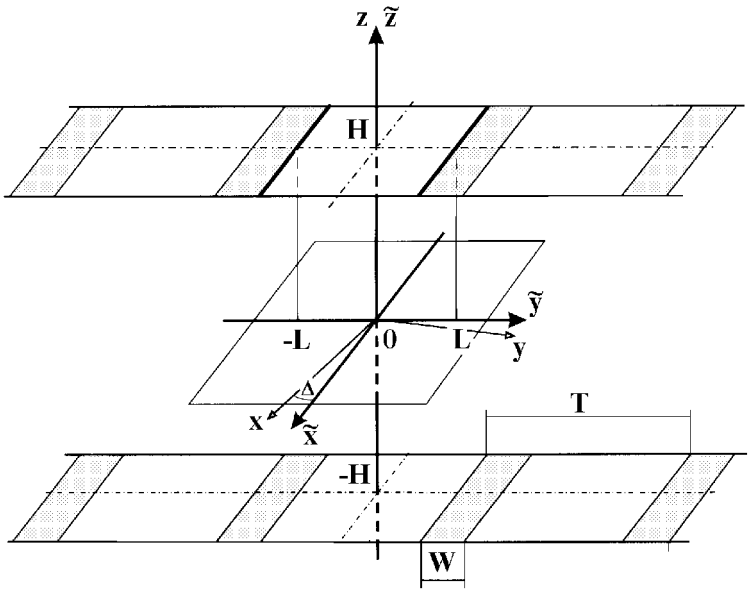

Figure 3. Schematic view of charge structure described in the text. $(\tilde{x}, \tilde{y}, \tilde{z})$ is the local coordinate system centred at the rare-earth position, while the system (x, y, z) is related to the crystal lattice. Shadowed tapes in the planes $z = \pm H$ show the charged area. Bold lines at $y = \pm L$ are charged filaments. T and W denote tape period and width, respectively.

We assume the charge array to have a sufficiently high symmetry (at least orthorhombic) and consider local coordinate system $(\tilde{x}, \tilde{y}, \tilde{z})$ with the origin at the rare-earth ion and the electric charges located within two parallel planes at $\tilde{z} = \pm H$ (figure 3). The charge density uniformly extended in the $\tilde{x}$-direction is described by function $f(L)$ where L is the distance in the $\tilde{y}$-direction between the $\tilde{z}$-axis and a particular charged area.

Let us first consider the electrostatic potential generated by an infinite uniformly charged filament elongated in the $\tilde{x}$-direction. The perturbing crystalline potential of the filament acting on an f electron of the rare-earth ion at a point $(\tilde{x}, \tilde{y}, \tilde{z})$ is:

$$U(\tilde{x}, \tilde{y}, \tilde{z}) = U(\tilde{x}, \tilde{y}) = \xi \ln \frac{H^2 + L^2}{(H - \tilde{z})^2 + (L - \tilde{y})^2} \tag{2}$$

where ξ is the linear charge density. Taking into account that due to small f-shell radius $|\tilde{y}|$; $|\tilde{z}| \ll \sqrt{L^2 + H^2}$ and introducing the notations:

$$\alpha = \frac{\tilde{y}}{\sqrt{L^2 + H^2}} \qquad \beta = \frac{\tilde{z}}{\sqrt{L^2 + H^2}} \tag{3}$$

equation (2) can be presented as an expansion:

$$U(\tilde{x}, \tilde{y}) = \xi \sum_{p,q} F_{pq} \alpha^p \beta^q. \tag{4}$$

Owing to the selection rules for the matrix elements [33] only the terms of expansion (4) with $p + q = 2$, 4 and 6 contribute to the SH.

The potential due to a family of similar parallel filaments is given by the sum of individual contributions. Since we assume either tetragonal or orthorhombic symmetry, for each pair of symmetrical filaments located at (L_i, H) and $(-L_i, H)$, $i = 1, 2, 3, \ldots, N$ (figure 3) the terms in which α and β occur to an odd power cancel in the sum. As a result, the relevant part of the electric potential generated by the pair of the uniformly charged parallel filaments is†:

$$\begin{aligned} U(\tilde{y}, \tilde{z}) &= U_2 U(\tilde{y}, \tilde{z}) + U_4(\tilde{y}, \tilde{z}) + U_6(\tilde{y}, \tilde{z}) \\ U_2(\tilde{y}, \tilde{z}) &= 2\xi g_2(L, H)\{\tilde{z} - \tilde{y}^2\} \\ U_4(\tilde{y}, \tilde{z}) &= 2\xi g_4(L, H)\{\tilde{y}^4 - 6\tilde{y}^2\tilde{z}^2 + \tilde{z}^4\} \\ U_6(\tilde{y}, \tilde{z}) &= 2\xi g_6(L, H)\{(\tilde{z}^6 - \tilde{y}^6) - 15\tilde{y}^2\tilde{z}^2(\tilde{z}^2 - \tilde{y}^2)\} \end{aligned} \tag{5}$$

where

$$\begin{aligned} g_2(L, H) &= (H^2 - L^2/(H^2 + L^2)^2) \\ g_4(L, H) &= \tfrac{1}{2}(H^4 - 6H^2L^2 + L^4)/(H^2 + L^2)^4 \\ g_6(L, H) &= \tfrac{1}{3}\{(H^6 - L^6) - 15H^2L^2(H^2 - L^2)\}/(H^2 + L^2)^6. \end{aligned} \tag{6}$$

Factors g_2, g_4, g_6 describe the contribution from a single filament. The coefficient 2 stands in equation (5) to emphasize that the field in question is generated by the pair of filaments. For the system of four filaments located at (L, H), $(-L, H)$, $(L, -H)$, $(-L, -H)$, respectively, the coefficient 2 in (5) is replaced by a factor of 4. In the following we will use the notation *coordination number* K for this numerical factor. For the array of KN filaments:

$$\begin{aligned} U_2(\tilde{y}, \tilde{z}) &= KG_2\{\tilde{z}^2 - \tilde{y}^2\} \\ U_4(\tilde{y}, \tilde{z}) &= KG_4\{\tilde{y}^4 - 6\tilde{y}^2\tilde{z}^2 + \tilde{z}^4\} \\ U_6(\tilde{y}, \tilde{z}) &= KG_6\{\tilde{z}^6 - \tilde{y}^6 - 15\tilde{y}^2\tilde{z}^2(\tilde{z}^2 - \tilde{y}^2)\} \end{aligned} \tag{7}$$

where

$$G_n = \sum_{i=1}^{N} g_n^i(L_i, H) \qquad n = 2, 4, 6. \tag{8}$$

In spherical coordinates equations (5)–(8) transform to:

$$U(\tilde{y}, \tilde{z}) = \sum_{n,m} \tilde{A}_n^m r^n Y_n^m(\tilde{\vartheta}, \tilde{\varphi}) \qquad n = 2, 4, 6; m = 0, \pm 2, \pm 4, \ldots \pm n \tag{9}$$

where coefficients $\tilde{A}_n^m$ are as follows:

$$\tilde{A}_2^0 = KG_2 2\left(\frac{\pi}{5}\right)^{1/2} \qquad \tilde{A}_6^0 = KG_6 2\left(\frac{\pi}{13}\right)^{1/2}$$

† Naturally, the same result occurs for the pair located at (L, H), $(L, -H)$.

$$\begin{aligned}
&\tilde{A}_2^{\pm 2} = KG_2\left(\frac{\pi}{15}\right)^{1/2} \qquad \tilde{A}_6^{\pm 2} = KG_6 15\left(\frac{2\pi}{2730}\right)^{1/2} \\
&\tilde{A}_4^{0} = KG_4\frac{2}{3}(\pi)^{1/2} \qquad \tilde{A}_6^{\pm 4} = KG_6\frac{1}{7}\left(\frac{14\pi}{13}\right)^{1/2} \\
&\tilde{A}_4^{\pm 2} = KG_4\frac{2}{3}\left(\frac{2\pi}{5}\right)^{1/2} \qquad \tilde{A}_6^{\pm 6} = KG_6\frac{1}{231}\left(\frac{231\pi}{13}\right)^{1/2} \\
&\tilde{A}_4^{\pm 4} = KG_4\frac{1}{3}\left(\frac{2\pi}{35}\right)^{1/2}.
\end{aligned} \tag{10}$$

For the spherical harmonics Y_n^m we use the notations as defined by Hutchings [33].

In the coordinate system (x, y, z) related to the crystallographic axes of the lattice (figure 3), from equation (9) we obtain:

$$U(r, \vartheta, \varphi) = \sum_{n,m} A_n^m r^n Y_n^m(\vartheta, \varphi) = \sum_{n,m} \tilde{A}_n^m \, \mathrm{e}^{-\mathrm{i}m\Delta} r^n Y_n^m(\vartheta, \varphi) \tag{11}$$

where the coefficients $\tilde{A}_n^m$ are calculated with equations (10) in the local coordinate system $(\tilde{x}, \tilde{y}, \tilde{z})$. Δ is the azimuth angle between the coordinate systems. At $\Delta \neq (0, \pi/2)$ the coefficients A_n^m have imaginary parts.

Following the standard procedure [33, 34], the crystal-field Hamiltonian

$$\hat{H}_{cf} = -|e| \sum_i \hat{U}(x_i, y_i, z_i)$$

can be written in the form of operator equivalents:

$$\hat{H}_{cf} = \sum_n \sum_{m \geqslant 0} \sum_{\alpha} B_{nm}^{\alpha} \hat{O}_{nm}^{\alpha} \qquad \alpha = 0, c, s, \qquad n = 2, 4, 6; \qquad m \leqslant n \tag{12}$$

where $\hat{O}_{nm}^{\alpha}$ are the operator equivalents introduced by Stevens [34] and

$$B_{nm}^{\alpha} = -|e| \gamma_{nm}^{\alpha} k_{nm} \Theta_n \langle r^n \rangle \tag{13}$$

are the CEF parameters. Θ_n are the reduced matrix elements listed in [33]. $\langle r^n \rangle$ is the nth moment of the radial distribution of the 4f electrons [43]. The matrix of geometrical factors γ_{nm}^{α} for a series of parallel filaments is determined as follows:

$$\gamma_n^0 = \tilde{A}_n^0 \qquad \gamma_{nm}^c = \sqrt{2}\tilde{A}_n^m \cos(m\Delta) \qquad \gamma_{nm}^s = \sqrt{2}\tilde{A}_n^m \sin(m\Delta). \tag{14}$$

Taking into account equations (10), (13) and (14) we can write now explicit formulae for the parameters of the crystalline field generated by the array of infinite filaments (figure 3):

$$\begin{aligned}
&B_{20} = \tfrac{1}{2}b_2 \qquad B_{60} = \tfrac{1}{16}b_6 \\
&B_{22}^c = \tfrac{1}{2}\cos(2\Delta)b_2 \qquad B_{62}^c = \tfrac{15}{32}\cos(2\Delta)b_6 \\
&B_{22}^s = \tfrac{1}{2}\sin(2\Delta)b_2 \qquad B_{62}^s = \tfrac{15}{32}\sin(2\Delta)b_6 \\
&B_{40} = \tfrac{1}{8}b_4 \qquad B_{64}^c = \tfrac{3}{16}\cos(4\Delta)b_6 \\
&B_{42}^c = \tfrac{1}{2}\cos(2\Delta)b_4 \qquad B_{64}^s = \tfrac{3}{16}\sin(4\Delta)b_6 \\
&B_{42}^s = \tfrac{1}{2}\sin(2\Delta)b_4 \qquad B_{66}^c = \tfrac{1}{32}\cos(6\Delta)b_6 \\
&B_{44}^c = \tfrac{1}{8}\cos(4\Delta)b_4 \qquad B_{66}^s = \tfrac{1}{32}\sin(6\Delta)b_6 \\
&B_{44}^s = \tfrac{1}{8}\sin(4\Delta)b_4
\end{aligned} \tag{15}$$

$$b_n = -K|e|G_n\Theta_n\langle r^n \rangle \qquad n = 2, 4, 6 \tag{16}$$

where G_n are determined by equations (8).

For $\alpha = (0, c)$ one can use the Stevens operator equivalents listed in [33]. Expressions for the operators with $\alpha = s$ may be derived using, e.g. the following procedure. Let us take into account that spherical harmonics $Y_n^n; Y_n^{n-1}; \ldots; Y_n^{-n}$ themselves form a full set of irreducible tensor operators. Thus, according to Wigner–Eckart theorem combinations $\sum_i r_i Y_n^m$ can be substituted by a set of the equivalent tensor operators of the same rank:

$$\sum_i r_i^n Y_n^m(\vartheta_i, \varphi_i) \equiv \Theta_n \langle r^n \rangle \hat{W}_n^m. \tag{17}$$

Using the algorithm given in [44], one can choose an operator proportional to $\hat{J}_+^n$ as the equivalent tensor operator $\hat{W}_n^n$. Other operators of a full set can be obtained using the following recurrent formula:

$$[\hat{J}-; \hat{W}_n^m] = \sqrt{n(n+1) - m(m+1)}\,\hat{W}_n^{m-1}. \tag{18}$$

Introducing the definition $\hat{W}_n^n = (k_{nm}/\sqrt{2})\hat{J}_+^n$, one obtains the expressions for the diagonal operator equivalents:

$$\hat{O}_{22}^s = \frac{1}{2\mathrm{i}}\{\hat{J}_+^2 - \hat{J}_-^2\} \qquad \hat{O}_{44}^s = \frac{1}{2\mathrm{i}}\{\hat{J}_+^4 - \hat{J}_-^4\} \qquad \hat{O}_{66}^s = \frac{1}{2\mathrm{i}}\{\hat{J}_+^6 - \hat{J}_-^6\}. \tag{19}$$

For the off-diagonal operators the calculation yields:

$$\begin{aligned}
\hat{O}_{42}^s &= \frac{1}{2\mathrm{i}}\{\hat{J}_+^2(7\hat{J}_z^2 + 14\hat{J}_z - J(J+1) + 9) - \hat{J}_-^2(7\hat{J}_z^2 - 14\hat{J}_z - J(J+1) + 9)\} \\
\hat{O}_{62}^s &= \frac{1}{2\mathrm{i}}\{\hat{J}_+^2(33\hat{J}_z^4 + 132\hat{J}_z^3 - 18J(J+1)\hat{J}_z^2 + 273\hat{J}_z^2 - 36J(J+1)\hat{J}_z + 282\hat{J}_z \\
&\qquad + J^2(J+1)^2 - 26J(J+1) + 120) - \hat{J}_-^2(33\hat{J}_z^4 - 132\hat{J}_z^3 - 18J(J+1)\hat{J}_z^2 \\
&\qquad + 273\hat{J}_z^2 + 36J(J+1)\hat{J}_z - 282\hat{J}_z + J^2(J+1)^2 - 26J(J+1) + 120)\} \\
\hat{O}_{64}^s &= \frac{1}{2\mathrm{i}}\{\hat{J}_+^4(11\hat{J}_z^2 + 44\hat{J}_z - J(J+1) + 50) - \hat{J}_-^4(11\hat{J}_z^2 - 44\hat{J}_z - J(J+1) + 50)\}.
\end{aligned} \tag{20}$$

Equations (19) and (20) are symmetrical with respect to the permutation $\hat{W}_n^m \to -\hat{W}_n^{-m}$. Replacing the differences in these equations by corresponding sums and introducing the factors $1/2$ instead of $1/2\mathrm{i}$ one immediately obtains the expressions for the operators $\hat{O}_{nm}^c$ which coincide exactly with those from [33]. Thus, a full set of Stevens operators for all n and m is determined.

Equations (15) show that the specific 'filament-like' charge symmetry leads to the rigid relations between the CEF parameters of the same order independently of other details of the charge distribution. Indeed, derived expressions can easily be generalized for any two or three dimensional charge distribution, which is constant in a certain direction and obeys the symmetry $f(L) = f(-L)$†. In the two-dimensional case the linear charge density ξ in equation (5) must be replaced by $f(L)\,\mathrm{d}L$, so that the crystal-field potential of such a charged plane at a point $(\tilde{x}, \tilde{y}, \tilde{z})$ is determined by equations (7) but coefficients G_n are as follows:

$$G_n = G_n(H) = \int_0^\infty \mathrm{d}L f(L) g_n(L, H) = C_n \int_0^\infty \mathrm{d}\lambda f(H\lambda)\chi_n(\lambda) \qquad n = 2, 4, 6 \tag{21}$$

$$C_2 = \frac{1}{H} \qquad C_4 = \frac{1}{2H^3} \qquad C_6 = \frac{1}{3H^5} \tag{22}$$

$$\chi_2(\lambda) = \frac{1-\lambda^2}{(1+\lambda^2)^2} \qquad \chi_4(\lambda) = \frac{1-6\lambda^2+\lambda^4}{(1+\lambda^2)^4}$$

$$\chi_6(\lambda) = \frac{1-\lambda^6-15\lambda^2(1-\lambda^2)}{(1+\lambda^2)^6}. \tag{23}$$

† Actually the distribution function $f(L)$ is determined up to any additive constant $f(L) + C$, since the uniformly charged infinite plane ($f(L) = \text{const}$ at $0 \leqslant L < \infty$) gives zero electrostatic potential at any point.

The dimensionless variable $\lambda = L/H$ is used for convenience. The functions $\chi_n(\lambda)$ act as weighting factors determining a relative contribution of the 'individual filament' located at $L = H\lambda$ to the crystal-field potential. $\chi_n(\lambda)$ are oscillating functions, both the 'oscillation frequency' and the damping rate being different for different orders.

For applications it is useful to consider a particular case of a tape-like charge distribution given by a series of KN rectangular 'impulses' with constant charge density Q_i for each impulse (figure 3), i.e.:

$$f(L) = Q_i \qquad \text{for } L_i \leqslant L \leqslant L_i + W_i \qquad i = 1, 2, \ldots, N$$
$$f(L) = 0 \qquad \text{for } L_i + W_i < L < L_{i+1}$$

where L_i is the y-coordinate of the ith 'impulse' front and W_i is its width. In this case equation (21) transforms into:

$$G_n = \sum_{i=1}^{N} G_n^i \qquad G_n^{(i)} = Q_i C_n \{\nu_n(\beta_i) - \nu_n(\alpha_i)\} \tag{24}$$

where C_n are determined by equation (22) and

$$\nu_2(\lambda) = \frac{\lambda}{1+\lambda^2} \qquad \nu_4(\lambda) = \frac{\lambda(3-\lambda^2)}{3(1+\lambda^2)^3} \qquad \nu_6(\lambda) = \frac{\lambda(5-10\lambda^2+\lambda^4)}{5(1+\lambda^2)^5} \tag{25}$$
$$\lambda = \{\alpha, \beta\} \qquad \alpha_i = \frac{L_i}{H} \qquad \beta_i = \frac{L_i + W_i}{H}$$

α and β being the values of variable λ corresponding to the impulse edges. Equations (15), (16), (24) and (25) determine the crystal-field parameters B_{nm} for an array of KN charged tapes. For the periodic array of equal tapes the values of variable λ for the tape edges are:

$$\alpha_i = \frac{\mathrm{i}T - (T+W)/2}{H} \qquad \beta_i = \frac{\mathrm{i}T - (T-W)/2}{H} \tag{26}$$

where T and W are the period and width, respectively, of the charged tape with constant charge Q (positive for holes and negative for electrons, in units of $|e|$ Å^{-2} where e is the electron charge). Equations (16), (24) and (26) lead to the following relations for the parameters b_n (in eV):

$$b_2 = -14.4 \times 4 \times Q \frac{\langle r^2 \rangle \Theta_2}{H} \left[\sum_{i=1}^{N} \{\nu_2(\beta_i) - \nu_2(\alpha_i)\} \right]$$
$$b_4 = -14.4 \times 4 \times Q \frac{\langle r^4 \rangle \Theta_4}{2H^3} \left[\sum_{i=1}^{N} \{\nu_4(\beta_i) - \nu_4(\alpha_i)\} \right] \tag{27}$$
$$b_6 = -14.4 \times 4 \times Q \frac{\langle r^6 \rangle \Theta_6}{3H^5} \left[\sum_{i=1}^{N} \{\nu_6(\beta_i) - \nu_6(\alpha_i)\} \right].$$

Here $\nu_n(\lambda)$ are given by equations (25), coordination number $K = 4$ is taken into account and all lengths are in angströms. The crystal-field parameters B_{nm} can be calculated with equations (15). Figure 4 represents a typical behaviour of the CEF parameters for positive charge of the tapes. Note that we consider the case of figure 3, i.e. there is no positively charged area exactly above/below the rare-earth position. For the small width ($T/W \gg 1$) the contribution to the second-order CEF parameters (they are equal for $\Delta = 0$) is positive at $L/H > 1$ and decreases with increase of L/H. As soon as T/W decreases (wide tapes) the contributions coming from the first members of a series become negative. The change of the sign results from the strict requirement to obey an asymptotic behaviour $B_{20} \to 0$ at $N \to \infty$ in the limit $W \to T$. For $L/H > 4$ the partial contribution to B_{2m} is a monotonic function of

T/W. The fourth-order parameters show non-monotonic behaviour as a function of T/W at small L/H with a maximum at $T/W \approx 1.5$. B_{6m} have a maximum at $T/W \approx 1.3$ but they are negative for narrow tapes. The contributions to both B_{4m} and B_{6m} vanish at $L/H > 3$. For a negative charge of tapes all B_{nm} in figure 4 have the opposite sign. Since the solution of equations (15) and (27) must be invariant with respect to any additive constant background, the behaviour of CEF parameters in figure 4 corresponds also to a sequence of negatively charged tapes with the same period T, width $(T - W)$, and shifted by $(T - W)/2$ along the y-axis with respect to the point $(x, 0, H)$. Therefore, to obtain a positive contribution to B_{20} for an infinite crystal doped with holes one has to consider the case of figure 3.

To take into account a finite length of charged tapes let us consider the expressions for the crystal-field parameters B_{nm} in the point-charge approximation. For example (for more details see [33], p 241),

$$\begin{aligned} B_{20} &= -|e|\frac{1}{4}\Theta_2\langle r^2\rangle \sum_j q_j \frac{3Z_j^2 - R_j^2}{R_j^5} \\ B_{22}^c &= -|e|\frac{3}{4}\Theta_2\langle r^2\rangle \sum_j q_j \frac{X_j^2 - Y_j^2}{R_j^5} \\ B_{22}^s &= -|e|\frac{3}{4}\Theta_2\langle r^2\rangle \sum_j q_j \frac{2X_jY_j}{R_j^5} \end{aligned} \tag{28}$$

where the summation is over ligand charges. Obviously, the second-order CEF parameters require a maximal correction, while for the higher orders it can safely be neglected. For the filament charge structure of figure 3 (angle $\Delta = 0$) substitution $q_j \to \xi\,\mathrm{d}x$ and transformation of equations (28) to integral yields:

$$\begin{aligned} B_{20} &= -|e|\xi\Theta_2\langle r^2\rangle \frac{1}{2}\frac{\sin\varphi_0}{(H^2+L^2)^2}\{(H^2 - L^2) + H^2\cos^2\varphi_0\} \\ B_{22}^c &= -|e|\xi\Theta_2\langle r^2\rangle \frac{1}{2}\frac{\sin\varphi_0}{L^2+H^2}\left\{\sin^2\varphi_0 - \frac{L^2}{L^2+H^2}(3 - \sin^2\varphi_0)\right\} \\ \varphi_0 &= \arctan\frac{D}{\sqrt{H^2+L^2}} \end{aligned} \tag{29}$$

where D is the filament half-length. For an infinite filament $\varphi_0 = \pi/2$. If $D \gg (H^2 + L^2)^{1/2}$, expansion of equations (29) using $(H^2 + L^2)^{1/2}/D$ as a small parameter leads to the following relations:

$$\begin{aligned} B_{20} &= B_{20}(\infty)\left\{1 - \frac{1}{3}\frac{H^2+L^2}{L^2-H^2}\frac{H^2+L^2}{D^2}\right\} \\ B_{22}^c &= B_{22}^c(\infty)\left\{1 + \frac{3}{2}\frac{H^2+L^2}{L^2-H^2}\frac{H^2+L^2}{D^2}\right\} \end{aligned} \tag{30}$$

where the sign ∞ stands for an infinite filament length. Equations (30) show that at $L = 0$ the correction turns out to be less than 1% if the ratio $D/H > 10$. At $L/H \approx 5$ the same is true for $D/H > 50$ but in this case the absolute contribution to the second-order parameters becomes less important (see figure 4). We conclude therefore that at $D/H > 10$ the formulae derived for an infinite length of charge structure can be applied for a finite tape length.

4. Doping dependence of the CEF in $ErBa_2Cu_3O_x$ and $HoBa_2Cu_3O_x$

In order to apply the model of the extended planar charge structure to the Er-'123' copper oxide we proceed as follows. Let us assume that all nine CEF parameters are known for the undoped

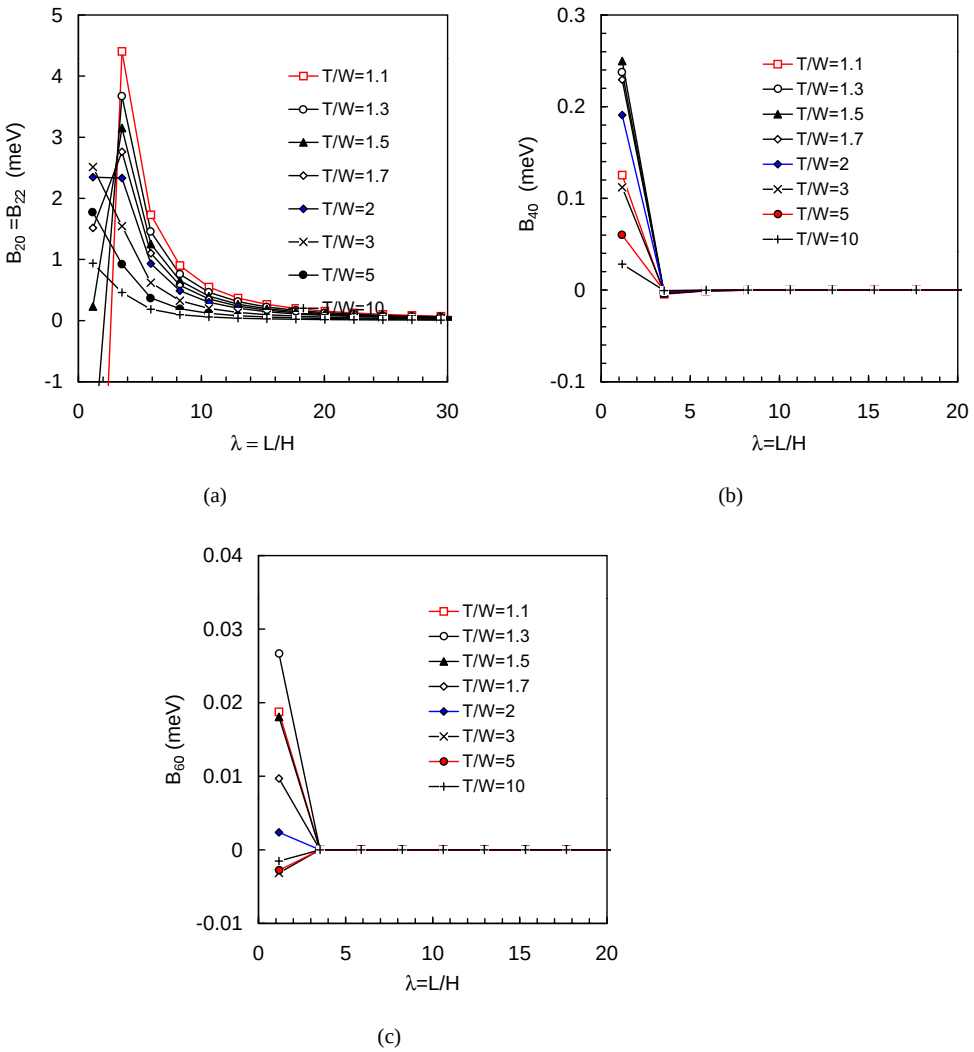

Figure 4. Dependence of the (a) second-, (b) fourth- and (c) sixth-order CEF parameters B_{n0} on variable λ calculated with equations (15) and (27) for the tape charged structure (figure 3). The values of λ correspond to the centre of the tape, $H = 1.4$ Å, $n = +0.0087\,|e|$ Å^{-2}.

sample from the experiment [31] and calculate their variation due to the hole doping in terms of our model. We consider the simplest case of charge geometry given by the periodic array of equal charged tapes with coordination number 4 (equations (27)). The separation between the rare-earth site and the CuO_2 planes $H = (z - 0.5)c$ was calculated for each oxygen content using the structural data from [31] (c is the crystal lattice parameter, and z is the z-coordinate of Cu(2) sites). Indeed, there is no great choice for T. The period should coincide with the crystal lattice parameter along the ab-plane since the experiment shows sharp CEF transitions without any substructure for the sample with $x = 6.98$. We neglected the variation of the in-plane lattice parameters for $ErBa_2Cu_3O_x$ with x and fixed the period of the tapes at $T = 3.85$ Å (the mean value of the in-plane lattice parameters). Since the experiment reveals all the leading CEF parameters to increase due to the hole doping, positively charged tapes cannot be set

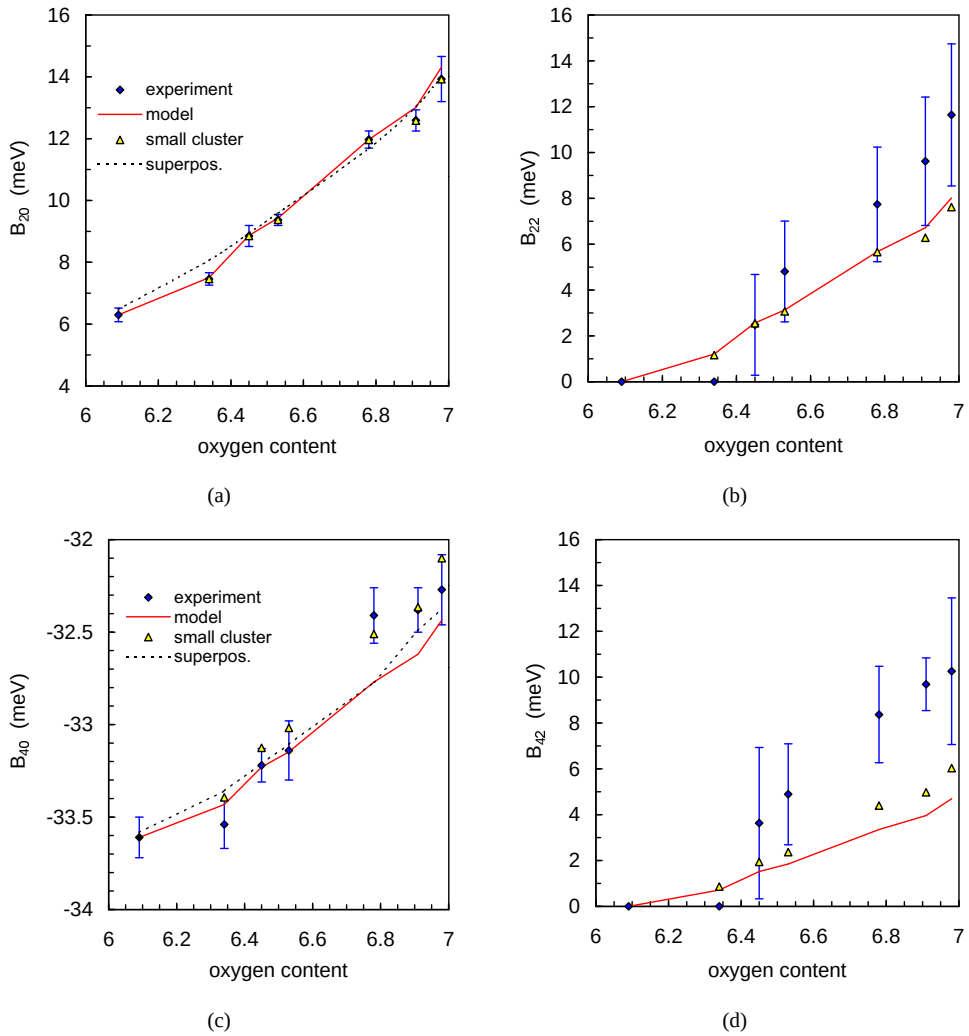

Figure 5. (a)–(g) Doping dependence of the CEF parameters for $ErBa_2Cu_3O_x$. (h) Hole concentration n as a function of oxygen content x for $ErBa_2Cu_3O_x$ derived to describe the variation of the CEF parameters in terms of equations (27). Experimental values of B_{nm} are taken from [31]. Notations 'model' and 'small cluster' correspond to the case of $N \to \infty$ (an infinite biplane) and $N = 3$, respectively. Model parameters W and Q for $N \to \infty$ are given in table 2. $W = 1.73$ Å for $N = 3$. Notation 'superpos' corresponds to the weighted values of n and B_{nm} calculated with equations (31) and (32), respectively.

above/below the rare-earth site (see section 3). This means that the tapes can be directed along the a- or b-direction but never along $(0, \pm 1, \pm 1)$, i.e. the angle $\Delta = 0$. Therefore, there are only two model parameters $W < T$ and Q to be found from a comparison with the experiment. Following [39], corrections for the nth moments of the radial distribution of the 4f electrons were taken into account by replacing $\langle r^n \rangle (1 - \sigma_n)/\tau^n$ for $\langle r^n \rangle$ in equations (27), where σ_n and τ^n are parameters which depend only on the number of 4f electrons of the R ion.

Figure 5 shows the result of fitting in the limit of an infinite crystal, $N \to \infty$. Only a single biplane is considered. The values of W and Q are given in table 2. n in table 2 is

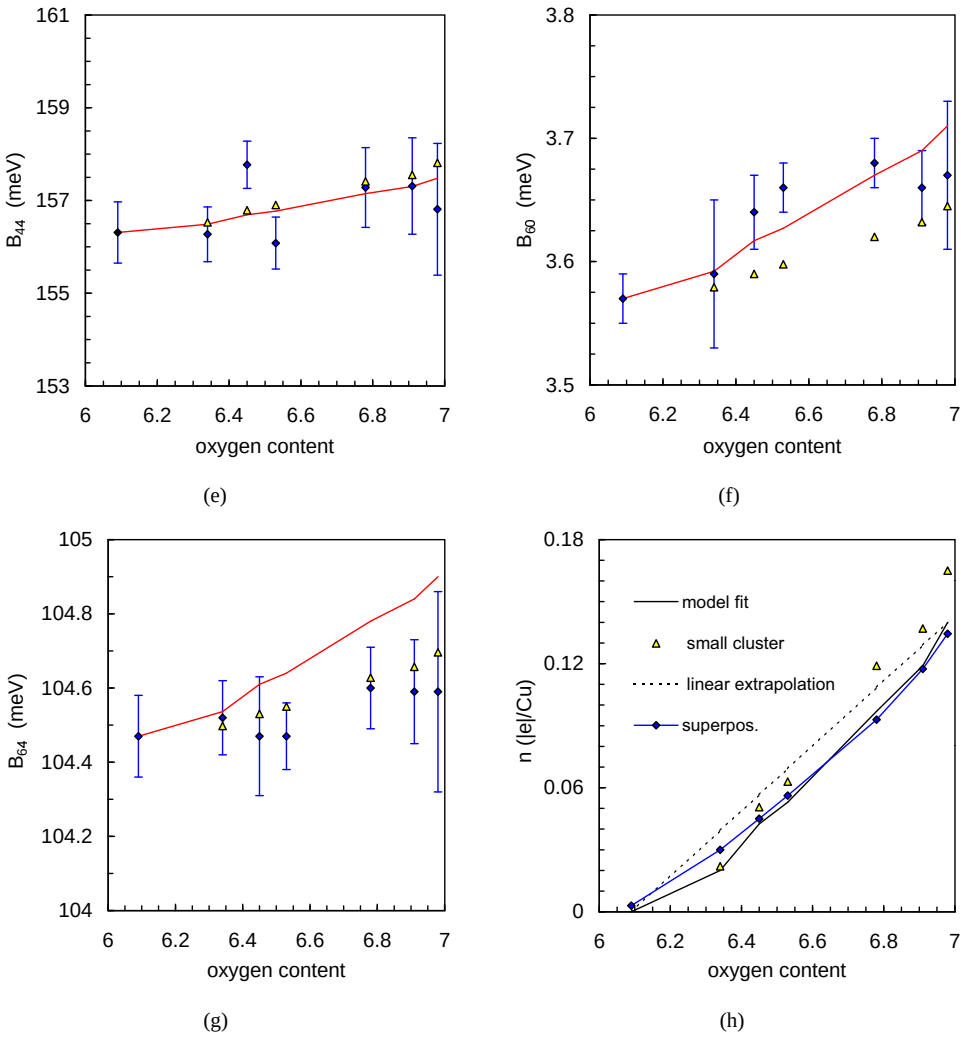

Figure 5. (Continued)

the hole concentration per CuO_2 block, calculated as $n = (Q) \times$ (lattice parameter along the tape direction) $\times$ (W). We conclude thus that (i) all the leading CEF parameters are found to be well described by the suggested model. (ii) The hole concentration $n \approx 0.14(|e|/\mathrm{Cu})$, required to describe variation of the CEF parameters going from $x = 6$ to $x = 7$, is in excellent agreement with the previous CEF analysis in terms of equation (1) [31] and other experiments [37]. (iii) The model describes reasonably well not only the leading 'tetragonal' CEF parameters, but provides also a good approximation for the 'orthorhombic' parameters, with the exception of the sixth-order ones. However, the experimental uncertainty for these parameters is rather large. Note, that in the case of a charge net (tapes along the a- and b-directions of the lattice) the resulting CEF parameters B_{nm} should be calculated as a sum of two contributions $b_n(\Delta)$ with the angle $\Delta = 0$ and $\pi/2$, respectively. As a result the orthorhombic parameters decrease. For example, they vanish for the tetragonal tape lattice (as they should due to charge symmetry).

Table 2. CEF parameters B_{nm} (in meV) for $ErBa_2Cu_3O_x$ calculated with equations (27). The values of B_{nm} for the undoped sample are taken from [31] for $x = 6.09$. An infinite CuO_2 biplane around the Er^{3+} ion is considered.

(n, m)	$x = 6.09$	$x = 6.34$	$x = 6.45$	$x = 6.53$	$x = 6.78$	$x = 6.91$	$x = 6.98$
(2, 0)	6.3	7.50	8.87	9.43	11.97	13.02	14.31
(2, 2)	0	1.20	2.57	3.13	5.67	6.72	8.01
(4.0)	−33.61	−33.43	−33.23	−33.15	−32.77	−32.62	−32.44
(4, 2)	0	0.71	1.52	1.85	3.35	3.96	4.70
(4.4)	156.31	156.49	156.69	156.77	157.15	157.30	157.48
(6, 0)	3.57	3.59	3.62	3.63	3.67	3.69	3.71
(6, 2)	0	0.17	0.36	0.43	0.79	0.93	1.08
(6, 4)	104.47	104.54	104.61	104.64	104.78	104.84	104.90
(6, 6)	0	0.011	0.023	0.029	0.052	0.062	0.072
W (Å)		2.3	2.3	2.3	2.3	2.3	2.28
Q		0.0022	0.0048	0.006	0.011	0.0134	0.0159
n		0.020	0.043	0.053	0.097	0.119	0.140

To check the validity of the model several tests have been performed. First, it should be emphasized that the value of n is almost insensitive to the parameters W and Q. The uncertainty in the determination of these parameters from the fit can be estimated as ±5%. If W decreases, Q should be increased to achieve an initial convergence of the fit to the experimental values, and *vice versa*. Hence, in terms of the simplified charge geometry the width of tapes is unchanged under doping. Also, this simplification could explain why the model does not reproduce the behaviour of the sixth-order 'orthorhombic' parameters ($m = 2, 6$). In principle, corrections can be introduced to take into account the 'background' crystal-field parameters related to the ligand ions. This background varies with the oxygen concentration due to the structural modification. However, these corrections do not exceed ±1% for the 'tetragonal' fourth- and sixth-order parameters calculated in the point charge approximation for the nearest-neighbour oxygen shell with the structural parameters from [31].

The second test is to take into account the neighbouring CuO_2 biplanes. This contribution to B_{2m} is negative for small L/H and strongly suppressed by the higher absolute value of H. As a result of these two circumstances the correction to B_{2m} is as small as 2 to 3%. The fourth- and sixth-order parameters are absolutely insensitive to the neighbouring planes.

The size of a cluster is the third important factor. Until now we have discussed an infinite cluster. However, the result does not change significantly if only a narrow cluster (along the y-axis) is considered. For example, for $N = 3$ (i.e. the width of the cluster along the y-axis is about 20 Å) the best solution is found at $W = 1.73$ Å giving $Q = 0.0249$ ($|e|$ Å^{-2}), i.e. $n = 0.17$ ($|e|$/Cu) for $x = 6.98$ (figure 5). Agreement with the experiment is even better than in the case of an infinite cluster. Again, the nearest CuO_2 biplanes have negligible influence on all CEF parameters. More essential correction for the second-order parameters results from the finite length of the tapes along the x-axis. According to equation (30), if the tape length is more than 30–40 Å, these corrections do not exceed a few per cent.

The last test is related to the direct effect of the chain oxygen. As we saw above the influence of the chain oxygen is negligible in terms of the point-charge model. Our model provides an extra possibility to check whether the oxygen incorporation into the chain position has only a small effect on the CEF interaction at the rare-earth site. Indeed, the electrostatic potential due to a charged filament decreases slowly with distance as compared to the point charges (logarithmic decay instead of $1/r$). This means that the effect of the chain oxygen calculated in terms of our model by far exceeds the result expected for a point

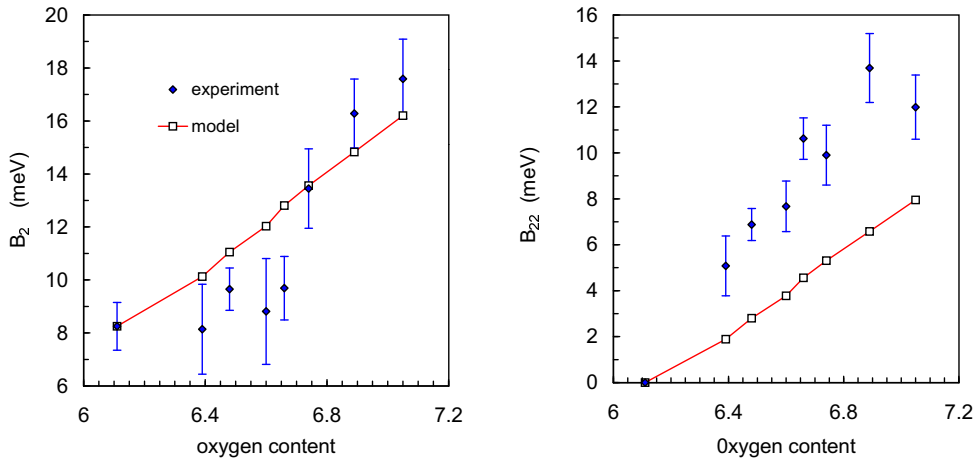

Figure 6. Doping dependence of the CEF parameters (a) B_{20} and (b) B_{22} for $HoBa_2Cu_3O_x$. Experimental values are taken from [35]. Model parameters W and $Q(x)$ (and, hence, hole concentration n) are the same as in the case of Er-'123' in the limit of $N \to \infty$.

charge. Taking $H = c/2$, where c is the lattice parameter, and assuming $W = 2.3$ Å we obtain corrections of the order of 2.5% for B_{2m} and less than 0.1% for B_{4m} and B_{6m} from the requirement $n = -2$ ($|e|$/cell) (i.e. chain oxygen is allowed to be spread along the a-axis; the value of W is the same as in table 2 for clarity).

In the model of charged tapes the 'orthorhombic' CEF parameters naturally arise as a direct consequence of the orthorhombic charge structure in the CuO_2 planes. However, we cannot state that this result is in favour of the model since in the case of Er-'123' the 'orthorhombic' parameters do not play an important role in the determination of the CEF spectra. They are additional fitting parameters used to improve fitting of the calculated spectra to the measured ones. In $HoBa_2Cu_3O_x$ the CEF spectrum turns out to be very sensitive to the B_{22} parameter [35]. The reason is that the $^5I_8$ ground state multiplet of Ho^{3+} is split into nine singlets and four doublets by the tetragonal crystal field at $x = 6$ (for Er^{3+} all CEF levels are Kramers doublets). The transition into the orthorhombic phase causes an additional splitting of the level scheme so that all CEF levels become singlets. Evidently, not only the energy levels but also the transition intensities depend on an orthorhombic distortion. As a result, in order to properly fit the observed CEF spectra for different x it is necessary to accurately adjust the B_{22} parameter as well. Figure 6 shows that the model under consideration reproduces the experimental behaviour of the second-order CEF parameters for Ho-'123' rather well. It should be emphasized that the model results in figure 6 represent not a fitting but straightforward recalculation of the data obtained for Er (table 2) for the case of Ho. We conclude that equations (27) are able to describe the doping dependence of the CEF spectra in $RBa_2Cu_3O_x$ with R = Er, Ho, i.e. the behaviour of nine *a priori* independent CEF parameters for each system, using only two fitting parameters, the values of which are equal for both compounds.

Figure 5 shows that the x-dependence of the CEF parameters follows the x-dependence of the hole concentration in the CuO_2 planes. Our model is able to explain why these dependences are nonlinear. We demonstrated above that the model allows us to consider small clusters formed by the CuO_2 biplane with a typical size of the order of a few lattice constants. This means that any doped hole can form a short charged tape in its local surroundings. This leads to

the corresponding variation of all the CEF parameters described by equations (27). Following [32], let us assume that only three types of local regions are allowed to exist, namely, undoped (this corresponds to $x = 6.0$), intermediately doped ($x = 6.5$) and highly doped ($x = 6.98$). In the ideal case of homogeneous charge distribution the hole concentration n is proportional to x, so that $n = 0$, 0.07 and 0.14 ($|e|$/Cu) for $x = 6.09$, 6.5 and 7.0, respectively. The averaged hole concentration $\langle n(x)\rangle$, given in table 2 for the integrated CEF spectra, obeys a simple law driven by statistical probabilities to find the corresponding local arrangements of the rare-earth ion. These probabilities P_i ($i = 0, 1, 2, 3, 4$) were introduced by P Allenspach *et al* [45] to describe the relative intensities of the spectral components of the CEF spectra in high-T_c copper-oxides. Later they were comprehensively used by J Mesot *et al* [32] and W Henggeler *et al* [46] to point out a percolative origin of the insulator–superconductor transition in Er-'123' and $Pr_{2-x}Ce_xCuO_{4-\delta}$, respectively. Using the definition of [32], the averaged hole concentration $\langle n(x)\rangle$ for $ErBa_2Cu_3O_x$ as a function of x can be written as:

$$\langle n(x)\rangle = n(x = 6.5)[(P_2(x) + P_3(x)] + n(x = 7.0)P_4(x). \tag{31}$$

The weighted CEF parameters which determine the integrated CEF spectrum are as follows:

$$B_{nm}^{obs}(x) = B_{nm}[n(6.0)][P_0(x) + P_1(x)] + B_{nm}[n(6.5)][P_2(x) + P_3(x)] + B_{nm}[n(7.0)P_4(x)]. \tag{32}$$

Indeed, the observed CEF parameters follow equation (32) rather well (figures 5(a) and 5(c)). Figure 5(h) shows the averaged hole concentration $\langle n(x)\rangle$ calculated according to equation (31) which clearly explains identical (and nonlinear) x-dependence of the CEF parameters (figure 1(b)). Therefore, not only a separation of the CEF spectra into different local components but the x-dependence of the CEF parameters themselves gives clear evidence for the formation of clusters which make the system inhomogeneous.

5. Discussion

The model of extended charges allows us to directly relate the variation of the CEF interaction at the rare-earth site in '123' structure with the charges appearing in the CuO_2 planes due to doping. Note that we considered the simplest charge density distribution in the planes which is approximated by a step function. In principle, any more complicated distributions of the same symmetry may be taken into account. However, even the simplest distribution yields a reasonable result. The hole concentration derived from our calculations corresponds surprisingly well to the results of other experiments and theoretical estimations. It is also important that the model emphasizes orthorhombic distortions (i.e. the elongation of the CuO_4 square along one of the planar Cu–O bonds) as an intrinsic feature of the doping process which, as seen from the charge geometry, is accompanied by charge order in the CuO_2 planes.

In fact, the orthorhombic tape structure means that the O(2) and O(3) sites in the CuO_2 planes turn out to be non-equivalent with respect to the charge transfer under doping. This type of order may be called 'Z[O(2)] $\neq$ Z[O(3)]'. In other words, the holes introduced by doping with oxygen go preferably to one type of plane oxygen site, i.e. O(2) (along the a- axis of the crystal lattice) or O(3) (along the b-axis). Our model cannot distinguish between them. We may only assert that charged tapes are directed either along the a- or b-axis but never along the (0, $\pm$1, $\pm$1) direction (see section 4).

If orthorhombic distortions result from this type of charge arrangement in a unit cell one can assume the tetragonal–orthorhombic phase transition in '123' compounds to be driven by the same mechanism. The chain oxygen ordering along the b-axis of the lattice seems to be a consequence of this electronic transition. In its turn, the oxygen arrangement helps to stabilize

the long-range orthorhombic distortions introduced by the doped holes and leads to a three-dimensional structural phase transition, which, in this form, is typical of the '123'-systems only. At the same time the local distortions of the Cu–O polyhedra are thought to be a general feature of the doping process in all cuprates [23, 24, 26–29, 46, 47]. The model developed to explain the x-dependence of the CEF parameters in $RBa_2Cu_3O_x$ allows us to demonstrate a relation between the structural distortions due to the doping and the tetragonal–orthorhombic phase transition in terms of equation (32). According to [32] superconductivity at $T_c = 60$ K in '123' compounds occurs at the two-dimensional percolation threshold $P_2 + P_3 = 50\%$. If both transitions, structural and superconducting, have the same triggering mechanism, the former is expected to occur at the three-dimensional percolation threshold, say, between 20 and 30% [48]. Taking the same probability $P_2 + P_3$ as a measure of the volume fraction of the orthorhombically distorted (i.e. intermediately doped) regions we conclude that the structural phase transition occurs before the superconducting one at $6.2 < x < 6.3$, in agreement with the experiment [47].

Evidently, the periodic array of charge tapes under consideration has the same geometry as stripes which form antiphase domain walls between antiferromagnetically ordered spins in the CuO_2 planes (e.g., compare figure 3 of the present paper with figure 1 of [27]). More important, our model of the doping dependence of the crystal-field effects emphasizes the same characteristic features of layered oxides as a model of the charged stripes, namely, the real-space charge order in the CuO_2 planes as well as distortions of the planar Cu–O bonds due to doping. In addition, due to the local nature the CEF interaction displays the phenomenon of 'frustrated phase separation' [30, 32]. This phenomenon was also observed by other local probes such as Mössbauer [49], NMR [50] and μSR [51] experiments. Due to these similarities it seems attractive to identify the charge tapes responsible for the doping dependence of the CEF parameters with stripes. However, there are severe doubts that such an identification is possible. (i) Our model emphasizes the ordered charge arrangement in a unit cell. The width of charge tapes $W \approx a/2$ (a is the in-plane lattice parameter) is by order of magnitude less than the width of stripes which is about 15 Å [20, 22, 27–29]. In terms of our model any attempt to extend stripe width up to a few lattice constants would result in strong contradiction with the observed behaviour of the CEF parameters. It is not straightforward to complicate the model taking into account, for example, influence of domain walls. (ii) The phenomenon of 'frustrated phase separation' associated with a separation of the CEF spectra into different local components can hardly be identified with the ordered charged stripes. The former is associated with the occupation of the chain oxygen sites and is governed by the statistical probabilities [32, 45]. (iii) The CEF interaction measured by inelastic neutron scattering technique essentially 'feels' a static component of the charge potential associated with the CuO_2 planes. A dynamic component affects the width of the CEF excitations. It is difficult to believe in the universal static character of stripes independently of doping level. Although we doubt that direct identification of charged stripes and charge order of the type '$Z[\mathrm{O}(2)] \neq Z[\mathrm{O}(3)]$' can be justified, both phenomena may be strictly tied. At the same time other interpretations associated with generic properties of the doped 2D planes are not excluded. The origin of the charge distribution within a unit cell may be related to an ordering of the type CDW [10], Jahn–Teller polaron formation due to local distortions of the planar CuO_4 cluster [52], or to the properties of doped spin chains [11]. In any case, the model requires further experimental verification. Measurements of the CEF spectra by inelastic neutron scattering at temperatures well above T_c, in the deeply overdoped regime as well as for the macroscopically tetragonal high-T_c oxides (the rare-earth doped infinite-layer compounds seem to be good candidates for this test) are expected to provide new insight into the underlying physics. All these experiments are in progress.

6. Conclusion

For the first time we present a new empirical approach to describe the doping dependence of the crystal-field interaction in $RBa_2Cu_3O_x$ (R = Er, Ho) superconductors in terms of the periodic array of charged tapes in the CuO_2 planes. The model is able to explain the variation of the CEF parameters in Er- and Ho-based compounds with only two fitting parameters the values of which are the same for both materials. The hole concentration in the CuO_2 planes is derived as a function of oxygen stoichiometry and found to be in agreement with the expectations. It is shown that not only the fine structure of the CEF spectra but also the x-dependence of the crystal-field parameters themselves gives clear evidence for the formation of clusters in $RBa_2Cu_3O_x$ which make the system inhomogeneous. The geometry of the charge distribution required to obtain these results provides evidence for charge order in the CuO_2 planes of the type 'Z[O(2)] $\neq$ Z[O(3)]' where Z is the effective charge of the in-plane oxygen sites. This order is assumed to result from the holes which are injected into the planes and preferably occupy one sort of in-plane oxygen site, either O(2) or O(3). This causes orthorhombic distortions of the tetragonal crystal structure of an undoped compound. When the volume fraction of the orthorhombically distorted (i.e. intermediately doped) regions reaches the 3D percolation threshold the structural phase transition occurs. For a critical volume fraction of 50% the doped clusters form a 2D percolative network, and the system undergoes a transition from the insulating to the metallic, i.e. superconducting, state [32]. Therefore, both the transitions occurring in '123' compounds due to oxygen intercalation seem to have the same triggering mechanism related to the number of holes injected into the planes, the former being followed by the latter, as expected from the dimension arguments. We suggest that the charge order of the type 'Z[O(2)] $\neq$ Z[O(3)]' cannot directly be associated with the stripe structure although a relation between these phenomena is not excluded.

Acknowledgments

We thank A Furrer, P Allenspach, J Mesot, U Staub, W Henggeler, A Moskvin, M Teplov and M Eremin for helpful discussions. Financial support by the Russian Foundation for Basic research (project No 96-02-16699), the Swiss National Science Foundation (project No 7IP 050162.96/1) and Russian State Programmes 'Neutron investigation of matter' (projects Nos 96-104, 96-305) and 'Superconductivity' (project No 96-051) is gratefully acknowledged.

References

[1] Bednorz J G and Muller K A 1986 *Z. Phys.* B **64** 189
[2] Emery V J and Kivelson S A 1995 *Nature* **374** 434
[3] Salkola M I, Emerz V J and Kivelson S A 1996 *J. Supercond.* **9** 401
[4] Zaanen J and van Saaarloos W 1997 *Physica* C **282–287** 178
[5] Castro-Neto A H and Hone D 1996 *Phys. Rev. Lett.* **76** 2165
[6] Castellani C, di Castro C and Grilli M 1996 *J. Supercond.* **9** 413
[7] Hammel P S and Scalapino D J 1996 *Phil. Mag.* B **74** 523
[8] Pines D 1997 *Physica* C **282–287** 273
[9] Aleksandrov A S 1997 *Physica* C **282–287** 269
[10] Eremin I, Eremin M, Varlamov S, Brinkman D, Mali M and Roos J 1997 *Phys. Rev.* B **56** 11 305
[11] Dagotto E and Rice T M 1996 *Science* **271** 618
[12] Junod A, Erb A and Renner C *Proc. 1st Euroconf. on Anomalous Superconductors* ed P B Littlewood and G Varelogiannis *Physica* C, at press
[13] Loram J W, Mirza K A, Cooper J R and Liang W Y 1993 *Phys. Rev. Lett.* **71** 1740
[14] Batlogg B, Hwang H Y, Takigi H, Cava R J, Kao H L and Kwo J 1994 *Physica* C **235–240** 130

[15] Takigava M, Reyes A P, Hammel P C, Thomson J D, Heffner R H, Fisk Z and Ott K S 1991 *Phys. Rev.* B **43** 247
[16] Loeser A G, Chen Z-X, Dessau D S, Marshall D S, Park C H, Fornier P and Kapitulnik A 1996 *Science* **273** 325
[17] Ding H, Yokoya T, Campuzano J C, Takahashi T, Randeira M, Norman M R, Mochiki T, Kadovaki K and Giapintzakis J 1996 *Nature* **382** 51
[18] Basov D N, Timusk T, Dabrowski B and Jorgensen J D 1994 *Phys. Rev.* B **50** 3511
[19] Tallon J L, Cooper J R, de Silva P S I P N, Williams G V M and Loram J W 1995 *Phys. Rev. Lett.* **75** 4111
[20] Tranquada J M, Sternlleb B J, Axe J D, Nakamura Y and Uchida S 1995 *Nature* **375** 561
[21] Tranquada J 1998 *Physica* B **241–243** 745
[22] Aeppli G, Mason T E, Hayden S M, Mook H A and Kulda J 1997 *Science* **278** 1432
[23] Cheong S-W, Hwang H Y, Chen C H, Batlogg B, Rupp L W and Carter S A 1994 *Phys. Rev.* B **49** 7088
[24] Hammel P C, Reyes A P, Cheong S-W, Fisk Z and Schriber J E 1993 *Phys. Rev. Lett.* **71** 440
[25] Yamada K, Lee C H, Endoch Y, Shirane G, Birgeneau R J and Kastner M A 1997 *Physica* C **282–287** 85
[26] Kataev V, Rameer B, Vavilov A, Büchner B, Hücker and Borowski R 1998 *Phys. Rev.* B **58** R11 876
[27] Bianconi A, Valetta A, Perali A and Saini N L 1997 *Solid State Commun.* **102** 369
[28] Bianconi A, Lusignoli M, Saini N L, Bordet P, Kvik Å and Radaelli P G 1996 *Phys. Rev.* B **54** 4310
[29] Saini N L, Lanzara A, Bianconi A and Oyanagi H 1998 *Phys. Rev.* B **58** 11 768
[30] Mesot J and Furrer A 1997 *J. Supercond.* **10** 623
[31] Mesot J, Allenspach P, Staub U, Furrer A, Mutka H, Osborn R and Taylor A 1993 *Phys. Rev.* B **47** 6027
[32] Mesot J, Allenspach P, Staub U, Furrer A and Mutka H 1993 *Phys. Rev. Lett.* **70** 865
[33] Hutchings M T 1964 *Solid State Physics* vol 16, ed F Seitz and D Turnbull (New York: Academic) pp 227–73
[34] Stevens K W H 1952 *Proc. Phys. Soc.* A **65** 209
[35] Staub U, Mesot J, Guillaume M, Allenspach P, Furrer A, Mutka H, Bowden Z and Taylor A 1994 *Phys. Rev.* B **50** 4068
[36] Podlesnyak A, Kozhevnikov V, Mirmelstein A, Allenspach P, Mesot J, Staub U, Furrer A, Osborn R, Bennington S M and Taylor A D 1991 *Physica* C **175** 587
[37] Tallon J L, Bernhard C, Shaked H, Hitterman R L and Jorgensen J D 1995 *Phys. Rev.* B **51** 12 911
[38] Sternheimer R M 1966 *Phys. Rev.* **146** 140
[39] Morrison C A 1988 *Angular Momentum Theory Applied to Interactions in Solids (Lecture Notes in Chemistry 47)* ed G Berthier *et al* (Berlin: Springer) p 122
[40] Bobrovskii V I, Zhdakhin I L and Mirmestein A V 1993 *Fiz. Met. Metalloved.* **76** 6027
[41] Mirmelstein A *et al* 1992 *Physica* C **200** 337
[42] Lea K R, Leask M J M and Wolf W P 1962 *J. Phys. Chem. Solids* **23** 1381
[43] Taylor K N R and Darby M I 1972 *Physics of Rare Earth Solids* (London: Chapman and Hall) p 45
[44] Watanabe H 1966 *Operator Methods in Ligand Field Theory* (New York: Prentice-Hall)
[45] Allenspach P, Furrer A and Rupp B 1990 *Progress in High-Temperature Superconductivity* vol 21, ed V L Aksenov *et al* (Singapore: World Scientific) pp 318–23
[46] Henggeler W, Cuntze G, Mesot J, Klauda M, Saemann-Ischenko G and Furrer A 1995 *Europhys. Lett.* **29** 233
[47] Radaelli P G, Segre C U, Hinks D G and Jorgensen J D 1992 *Phys. Rev.* B **45** 4923
[48] Kirkpatrick S 1973 *Rev. Mod. Phys.* **45** 574
[49] Hodges J A, Bonville P, Imbert P and Jéhanno G 1991 *Physica* C **184** 259
[50] Teplov M A, Bakharev O N, Dooglav A V, Egorov A V, Eremin M V, Tagirov A G, Volodin A G and Zhdanov R S 1991 *Physica* C **185–189** 1107
[51] Niedermayer C, Bernhard C and Budnik J I 1995 *J. Magn. Magn. Mater.* **140–144** 1287
[52] Moskvin A S 1997 *Physica* C **282–287** 1807